Article:
Stockdale, G, Milani, G and Sarhosis, V orcid.org/0000-0002-8604-8659 (2021) Dynamic modelling structure of hinge-controlled masonry arches and 2D accelerations. International Journal of Masonry Research and Innovation, 6 (3). pp. 255-284. ISSN 2056-9459

https://doi.org/10.1504/IJMRI.2021.116191

Dynamic Modelling of Hinge-Controlled Masonry Arches and 2D Accelerations

Gabriel Stockdale[a]*, Gabriele Milani[a], Vasilis Sarhosis[b]

[a] Dept. of Architecture, Built Environment and Construction Engineering, Politecnico di Milano Piazza Leonardo da Vinci 32, 20133 Milan, Italy

[b] School of Civil Engineering, University of Leeds, LS2 9JT, UK

*Corresponding author: gabriellee.stockdale@gmail.com

Abstract.

Engineering efficiency is paramount for the introduction of novel systems and formats of analysis. This work extends an accessible and efficient analysis platform by combining the kinematic equilibrium approach of limit analysis with the single degree of freedom nature of a hinge-controlled masonry arch to perform dynamic modelling of applied two-dimensional acceleration vectors. Utilizing ideal conditions, minimum work-paths are formulated to describe the work required to drive the arch to collapse. Then assuming conservative work allows the formation of a spatial description of kinetic energy, and ultimately the establishment of the time domain for constant 2D accelerations. A dynamic time incremental analysis structure is then formulated based upon the assumption of constant acceleration for each time step. This dynamic model propagates the centroid displacement and kinetic energy through an applied acceleration sequence. Lastly, the dynamic model under ideal conditions is tested for validity through half-cycle collapse domain benchmark and the conservation of energy.

Keywords: Near-Real Time Analysis, Dynamic Analysis, Seismic Analysis, KCLC, masonry arch

This research did not receive any specific grant from funding agencies in the public, commercial, or not-for-profit sectors.

1 INTRODUCTION

In the modern era of structural design and analysis, where labor dominates cost, efficiency is of the upmost importance for the success of any structural system. This condition of efficiency becomes even more prominent with the introduction (or reintroduction) of novel structural systems that do not align themselves with the standard foundations of modern engineering. This need for efficiency in a new structural system is further exacerbated by the lack of practitioners familiar with the costs of its actual construction. The further the system deviates from the accepted standards of steel, reinforced concrete, and timber, the more challenging that introduction becomes.

The argument has been made that the masonry arch has the potential to be an advantageous structural system for modern structural design and construction through the technique termed Reinforced Stability Based Design (RSBD) (Stockdale, 2016). The principle idea of this design methodology is to isolate the compressive and tensile components of the system such that the reinforcement is only active after initiation of a controlled mechanism. Then by defining failure as the onset of the mechanism, safety can be quantitatively designed into the structure through the reinforcement. In this manner, material strengths becomes a secondary consideration, generalized element-based structural health monitoring systems can be established with no significant calibration delays, and the proven longevity of structural masonry can be capitalized upon (Stockdale, 2012; Angelillo, 2014; Tralli, Alessandri and Milani, 2014). Unfortunately, the analysis of the masonry arch does not fit into the linear elastic model that provides the foundation for modern engineering, and thus any chance of success depends upon the development of its own efficient and accessible model.

The theoretical introduction of RSBD also transitions the focus from assessment to control. By controlling the mechanism, the focus of evaluation no longer pivots around the assumption of the four-hinged mechanism or the attempt to establish the minimum condition. Rather the analysis can be directly applied to the defined condition. This formulated the novel approach to the static stability analysis of masonry arches through the development of a first-order assessment strategy and the Kinematic Collapse Load Calculator (KCLC) (Stockdale *et al.*, 2018; Stockdale and Milani, 2019). Both tools were developed from and for the structural design and analysis of hinge-controlled masonry arches. They utilize a kinematic equilibrium approach of limit analysis (LA) to calculate the load magnitude and hinge reaction values that establish equilibrium of a defined kinematic state. This is achieved by incorporating the loading condition into the standard equilibrium problem (i.e. the sum of forces and moments) as a variable. The solution set is then evaluated against the kinematic boundary conditions to establish admissibility.

This simple analysis structure and the KCLC have proven to be quite adaptable as well. The first adaptation was the incorporation of any drawn arch geometry (Stockdale and Milani, 2018). Then through the validation process with experimental results, non-ideal mechanisms resulting from the inclusion of static friction, the tensile capacity compensation requirements for establishing rigid elements between hinges, and the decomposition of gravity to model the tilting plane were incorporated (Stockdale, Sarhosis and Milani, 2019b). Static motion of the kinematic

system was added to address an experimentally observed finite hinge stiffness (Stockdale, Sarhosis and Milani, 2019a). The inclusion static motion revealed that under constant horizontal acceleration the arch maintains a kinematically admissible condition as it propagates towards collapse.

Maintaining kinematic equilibrium through the static propagation of the kinematic condition generates a minimum work. Assuming energy conservation releases the path dependence of this work. This generates the potential to directly expand the static analysis structure into a dynamic modelling one for the SDOF system.

The objective of this work is to develop and validate the work-path approach for the dynamic modelling of hinge-controlled masonry arches subjected to two-dimensional acceleration profiles. First, a brief overview of existing dynamic analysis strategies is presented in Section 2. Section 3 details the work-path and time-domain formulation for horizontal accelerations. Section 4 expands the analysis, work-path development and time-domain formulation to non-horizontal accelerations. Then through the assumption of constant acceleration per time step, the analysis procedure for motion and energy propagation are developed in Section 5. Section 6 then provides an initial validation of the approach through a combination of Oppenheim's half-cycle collapse and the conservation of kinetic energy (Oppenheim, 1992). Section 7 concludes this work.

2 SEISMIC MODELLING STRATEGIES

For the analysis of masonry arches as a whole there does exist a significant amount of research and experimental investigations aimed at the assessment of existing structures (Hendry, 1998; Tralli, Alessandri and Milani, 2014; Sarhosis, Santis and de Felice, 2016). As with all modern analyses, the dynamic analysis of masonry arches can be divided into two primary categories: analytical and numerical. The numerical approaches are further divided into two main categories: a) non-linear finite element method (FEM); and b) the distinct (or discrete) element method (DEM). The discontinuous nature of masonry prohibits modelling in the elastic continuum, thus requiring the non-linear analysis (Dimitri and Tornabene, 2015). The non-linear FEM approach has been successfully applied in dynamic cases, but it requires a high level of expertise to employ and is computationally expensive (Fanning *et al.*, 2005; Pelà, Aprile and Benedetti, 2009, 2013; Gaetani *et al.*, 2017). DEM originated to address rock engineering where continuity is absent and it has been successful at simulating the dynamic behavior of masonry structures as well (De Lorenzis, DeJong and Ochsendorf, 2007; DeJong, 2009; Dimitri, De Lorenzis and Zavarise, 2011; DeJong and Dimitrakopoulos, 2014; Dimitri and Tornabene, 2015; Sarhosis *et al.*, 2016). Like its non-linear FEM counterpart, DEM requires a high level of expertise and computational costs.

The analytical approaches used for the seismic analysis of masonry arches are known as limit analysis (LA). These LA approaches are also divided in two with the upper and lower bound theorems. Lower bound of LA defines stability by establishing the existence of a thrust line that lies entirely within the arch boundary. This thrust line analysis arises from Hooke's hanging

chain analogy and was solidified by Heyman's safe theorem (Heyman, 1969). Being bound by stability, the lower bound theorem has been utilized to impose static horizontal testing through tilting plane analysis, but is not structured for dynamic conditions (Huerta, 2005; DeJong, 2009). The upper bound theorem is also known as the kinematic theorem and it states that an arch will fail if a kinematically admissible mechanism exists that produces positive or zero work from external forces. Traditionally, this approach applies equivalent horizontal accelerations combined with an iterative approach to the principles of virtual work (for static analyses) to determine collapse, or virtual powers (for dynamic analyses) to define dynamic conditions (Oppenheim, 1992; Gilbert and Melbourne, 1994; Clemente, 1998). In the context of validations, DeJong's (DeJong, 2009) lower bound tilting plane analysis was found in good agreement with the upper bound results from both Clemente (Clemente, 1998) and Oppenheim (Oppenheim, 1992). Additionally, the kinematic theorem has been validated for lateral loading both numerically and experimentally (Ochsendorf, 2002; De Luca, Giordano and Mele, 2004; Alexakis and Makris, 2014; Dimitri and Tornabene, 2015; Stockdale, Sarhosis and Milani, 2019b).

The kinematic theorem is structured around the kinematic condition. This directly connects the analysis to the existence of a motion state. In fact, the four-hinged arch is by definition a single degree of freedom (SDOF) system. Beginning with the four-hinged mechanism, Oppenheim (Oppenheim, 1992) was able to formulate the exact equations of motion for this condition and use them to study the overturning of an arch during the first half cycle of motion due to a step impulse. This model was expanded by De Lorenzis et al. (De Lorenzis, DeJong and Ochsendorf, 2007) through the introduction of Housner's (Housner, 1963) assumptions on impact for single rocking blocks to the four-hinged arch model. Applying the same step impulse as Oppenheim (Oppenheim, 1992), De Lorenzis et al. (De Lorenzis, DeJong and Ochsendorf, 2007) both identified the second boundary associated with the collapse of the second half cycle and that it is the governing condition. This model was further expanded by Kollár and Ther (Kollár and Ther, 2019) by removing the four-hinge limitation and evaluating the mutli-degree of freedom motions that can exist in systems without hinge control.

Where existing strategies directly develop the equations of motion, use virtual powers or rely on complex FE or DEM analysis structures, this research utilizes the path independence of conservative work to define the change in position and kinetic energy for constant accelerations. By incrementing this process through the time step of an acceleration sequence, the dynamic description of a hinged-controlled arch is obtained.

3 Work-Path and Time Domain for Horizontal Accelerations

The dynamic analysis procedure is developed by establishing a time-displacement relationship for a defined mechanism-acceleration pair through the path independence of conservative work. This begins with combining kinematic equilibrium analysis and the SDOF motion of a four-hinged arch to generate a work-path. From the work path a spatial kinetic energy equation is obtained and then utilized to establish a time displacement relationship.

3.1 KINEMATIC EQUILIBRIUM

Kinematic equilibrium analysis is the standard equilibrium evaluation of statics but applied to a kinematic condition through the incorporation of a loading variable required to establish the defined condition. For each analysis, the equilibrium equation sets are established in matrix form

$$[BC]\{r\} = \{q\} \tag{1}$$

so the solutions to the reaction and loading variables, $\boldsymbol{r}$, can be easily obtained by multiplying the inverse on the balance matrix, $\boldsymbol{BC}$, with the constants vector, $\boldsymbol{q}$

$$\{r\} = [BC]^{-1}\{q\} \tag{2}$$

Therefore, the equilibrium evaluation is only dependent on the boundary conditions of the kinematic condition and the loading geometry. For instance, consider the kinematic arch loaded with a leftward horizontal acceleration of magnitude $\lambda_a g$ as shown in Figure 1. By defining rigid elements between hinges, the acceleration forces can be applied through force equivalence at the centroid of each element. Then summing the moments about hinges H_1, H_2 and H_3 for elements one, two and three respectively generates

$$[BC] = \begin{bmatrix} -1 & 0 & 1 & 0 & 0 & 0 & 0 & 0 & f_{g1} \\ 0 & 1 & 0 & -1 & 0 & 0 & 0 & 0 & 0 \\ 0 & 0 & -\Delta y_{2,1} & \Delta x_{1,2} & 0 & 0 & 0 & 0 & -f_{g1}\Delta y_{CM1,1} \\ 0 & 0 & -1 & 0 & 1 & 0 & 0 & 0 & f_{g2} \\ 0 & 0 & 0 & 1 & 0 & 1 & 0 & 0 & 0 \\ 0 & 0 & 0 & 0 & \Delta y_{3,2} & \Delta x_{2,3} & 0 & 0 & f_{g2}\Delta y_{2,CM2} \\ 0 & 0 & 0 & 0 & -1 & 0 & 1 & 0 & f_{g3} \\ 0 & 0 & 0 & 0 & 0 & -1 & 0 & 1 & 0 \\ 0 & 0 & 0 & 0 & 0 & 0 & \Delta y_{3,4} & -\Delta x_{3,4} & f_{g3}\Delta y_{3,CM3} \end{bmatrix} \tag{3}$$

and

$$\{q\} = [0 \quad f_{g1} \quad -f_{g1}\Delta x_{1,CM1} \quad 0 \quad f_{g2} \quad f_{g2}\Delta x_{2,CM2} \quad 0 \quad f_{g3} \quad -f_{g3}\Delta x_{3,CM3}]^T \tag{4}$$

for

$$\{r\} = [h_1 \quad v_1 \quad h_2 \quad v_2 \quad h_3 \quad v_3 \quad h_4 \quad v_4 \quad \lambda_a]^T \tag{5}$$

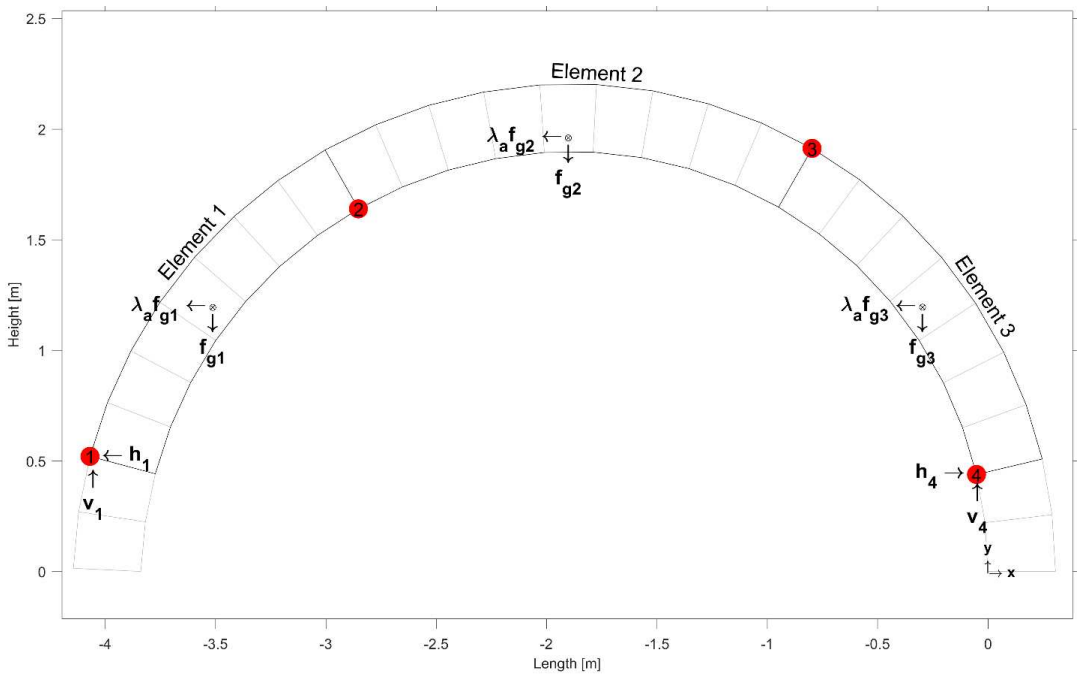

Figure 1. Kinematic equilibrium condition for leftward horizontal acceleration condition

For Eqns. 3 and 4, the subscripts of the vertical lever arms, Δy, and the horizontal lever arms, Δx, denote the hinges or center of mass locations used (i.e. $\Delta y_{3,4}$ is $(y_3 - y_4)$ and $\Delta x_{2,CM2}$ is $(x_2 - x_{CM2})$, ect.), and f_{gj} is the gravitational force of the j^{th} element. In Eqn. 5, h_i and v_i are the horizontal and vertical reactions at the i^{th} hinge respectively, and lastly, λ_a is the collapse load multiplier (in units of gravity, g) for the horizontal acceleration.

3.2 SDOF DEFORMATION

The hinge-controlled masonry arch can be described with three rigid elements connected by four pins with a motion bound by the rotation of the pins (see Figure 2). For a given rotation α_1 at H_1 (see Figure 2 for identifying lengths and angles), the rotation at H_4 is

$$\alpha_4 = \cos^{-1}\left(\frac{l_{12}}{l_{34}}[\cos(\theta_{12} + \alpha_1) - \cos(\theta_{12})] + \cos(\theta_{43})\right) - \theta_{43} \tag{6}$$

From the rotations of α_1 and α_4, the translations of hinges H_2 and H_3 are known and the polar change, γ_{23}, of length l_{23} can be determined

$$\gamma_{23} = \theta'_{23} - \theta_{23} \tag{7}$$

This allows the rotations of the intermittent hinges H_2 and H_3 to be calculated by

$$\alpha_2 = \alpha_1 + \gamma_{23} \tag{8}$$

and

$$\alpha_3 = \alpha_4 + \gamma_{23} \tag{9}$$

respectively.

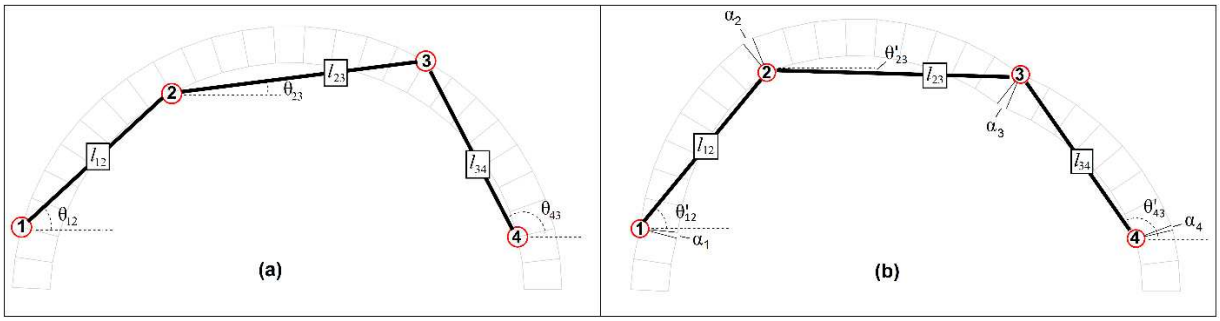

Figure 2. Rigid pin-connected length representation of the four-hinged arch mechanism in the (a) undeformed state and (b) after a deformation

3.3 KINEMATIC EQUILIBRIUM OF STATIC DEFORMATIONS

A custom KCLC was designed to incorporate the defined SDOF motion through the inclusion of a slider that defines the rotation angle of α_1. As with the hinge adjustment sliders, the equation set is evaluated for each adjustment to the rotation value. Figure 3 shows this custom KCLC with imposed α_1 rotations of 0°, 4°, 8°, and 12° imposed on the given arch-hinge-load-configuration. Note that the center of mass (CM) and the center of area (CA) are provided in addition to the collapse multiplier, hinge reactions and rotation values. This is to account for potential non-uniform block masses.

From the deformation sequence shown in Figure 3 there exists an admissible kinematic equilibrium condition through 11° of rotation at H_1. This deformation results in a capacity reduction of the collapse multiplier until the loss of admissibility. Also note the propagation of the CM is mapped for the deformation.

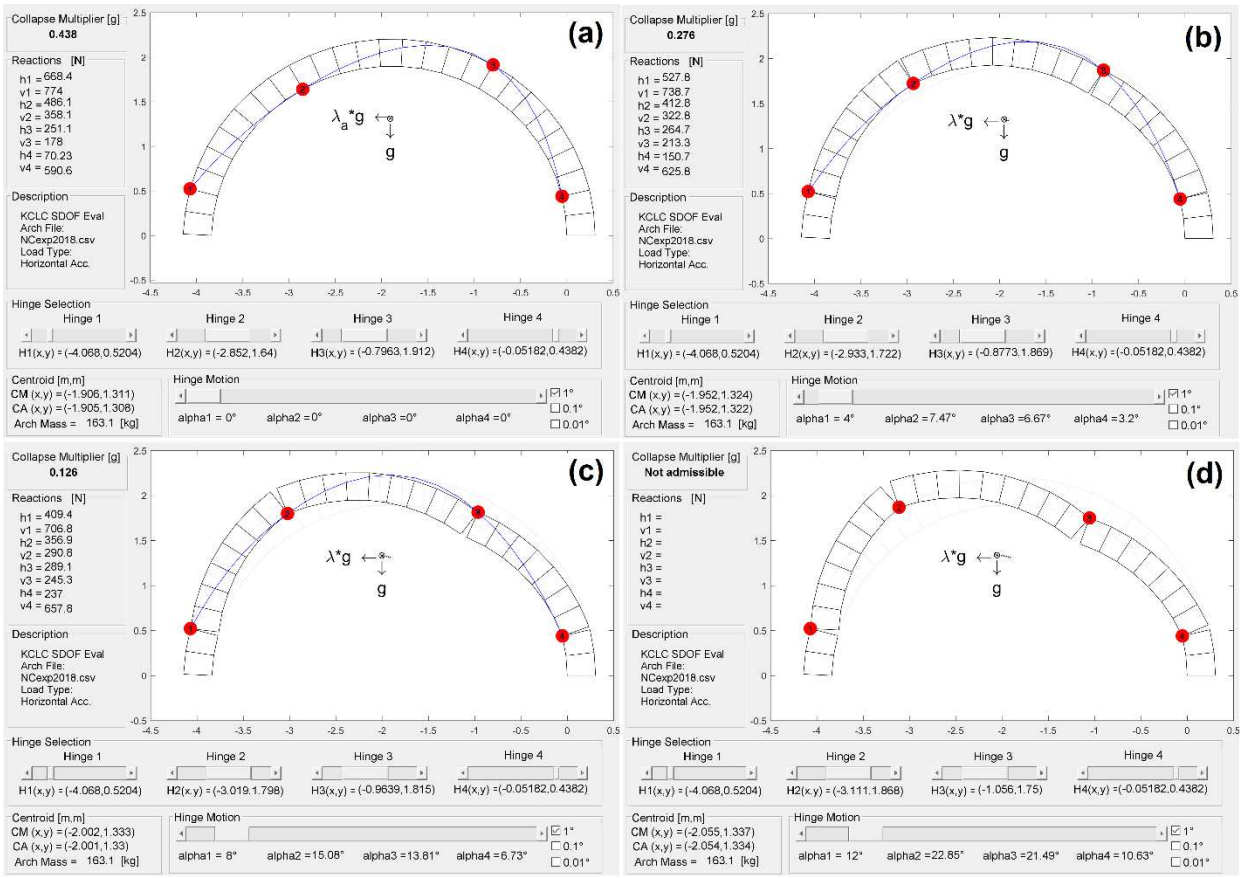

Figure 3. Custom KCLC with added hinge motion panel and centroid data display with applied α_1 rotations of (a) 0°, (b) 4°, (c) 8° and (d) 12°

3.4 EQUIVALENT SYSTEMS

For the imposed deformation sequence shown in Figure 3, the block, element, and full arch centroid positions were recorded for α_1 rotations between 0° and 12° with constant $\Delta\alpha_1$ of 0.1°. Through parametric plotting simplifications to the description of motion can be formulated. This allows the given condition of motion to be represented by single point translations and rotations.

3.4.1 Single Point Translations

Figure 4 shows this deformation path for the CM and a polynomial fit to the motion. The polynomial fit generates a simple deformation equation for the single point translation

$$y = A_1x^2 + A_2x + A_3 \tag{10}$$

with the constants A_i identified in Figure 4 for the condition shown in Figure 3.

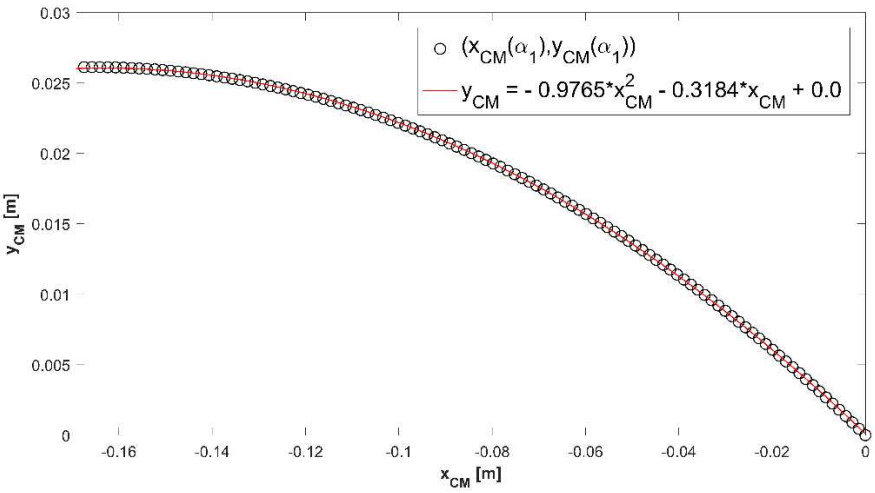

Figure 4. Parametric plot of the CM deformation path as a function of α_1 and 2nd order polynomial fit

3.4.2 Single Point Rotations

Point rotations must also be considered to account for the two-dimensional out of plane effects of motion being represented by a single point. These rotations are accounted for by the polar angles between the full arch centroid and the centroid of each of the rigid elements. Conservation of mass binds this relationship. Figure 5 shows the resulting rotation angles versus horizontal CM displacement for each element of the arch-hinge configuration in Fig. 3. Polynomial fits reveal reasonable representation by

$$\theta = B_1 x^2 + B_2 x + B_3 \tag{11}$$

for each element. The constants B_i, of Eqn. 11 are shown in Figure 5.

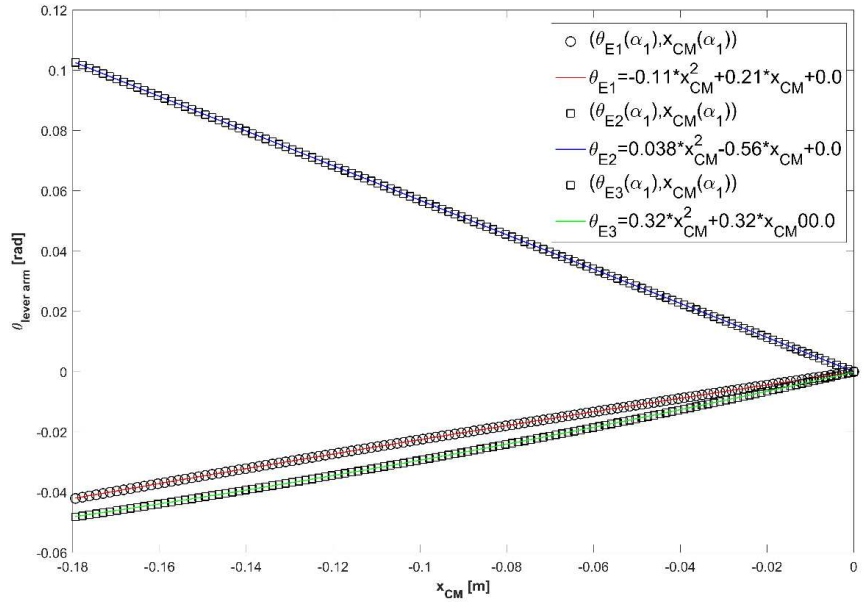

Figure 5. Parametric plots of the lever arm rotation angles versus horizontal CM displacement and the polynomial fits

3.5 Work Path and Potential Energy

The path independence of conservative work allows the use of the single point representation of mass and motion to establish work-paths related to the actual geometry of the hinge-controlled arch system. Figure 6 shows the acceleration force versus horizontal CM displacement for the single point. The out of plane contributions to work are obtained from considering the torque applied to the single point from each element's centroid and the rotation of the massless lever arms. Figure 7 shows the torque-rotation plots for each element. Also note that the sum of the torques maintains zero through the deformation sequence confirming equilibrium.

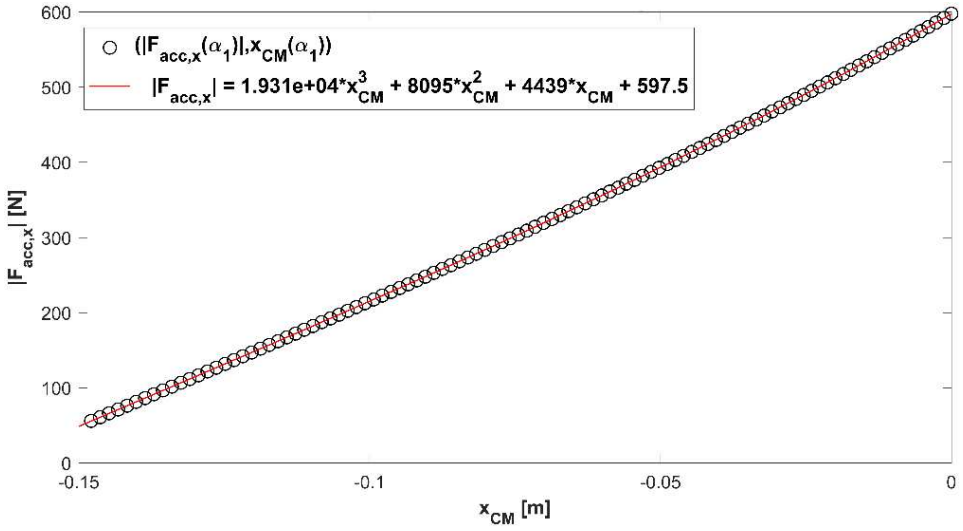

Figure 6. Parametric plot of acceleration force versus horizontal CM displacement and best fir polynomial

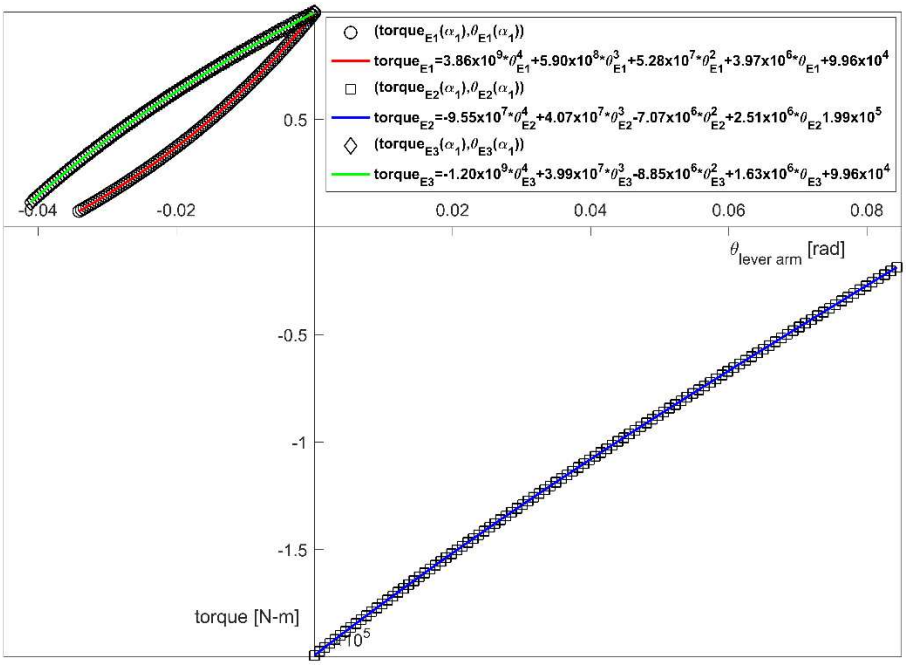

Figure 7. Parametric plot of the element induced torque at CM versus the respective lever arm rotation angles

The total work can be expressed as the sum of translational and rotational components

$$W = \int F dx + \int \tau_{E1} d\theta_{E1} + \int \tau_{E2} d\theta_{E2} + \int \tau_{E3} d\theta_{E3} \tag{12}$$

and integrating the force-displacement plot and torque rotation plots generates the work paths seen in Figure 8. The change in potential energy

$$\Delta PE = m_T g \Delta y \tag{13}$$

is also plotted in Figure 8. The work required to drive the arch to collapse is greater than the change in potential energy as a total and for the translational work alone. The excess translational work is the result of maintaining a thrust condition that supports the defined mechanism.

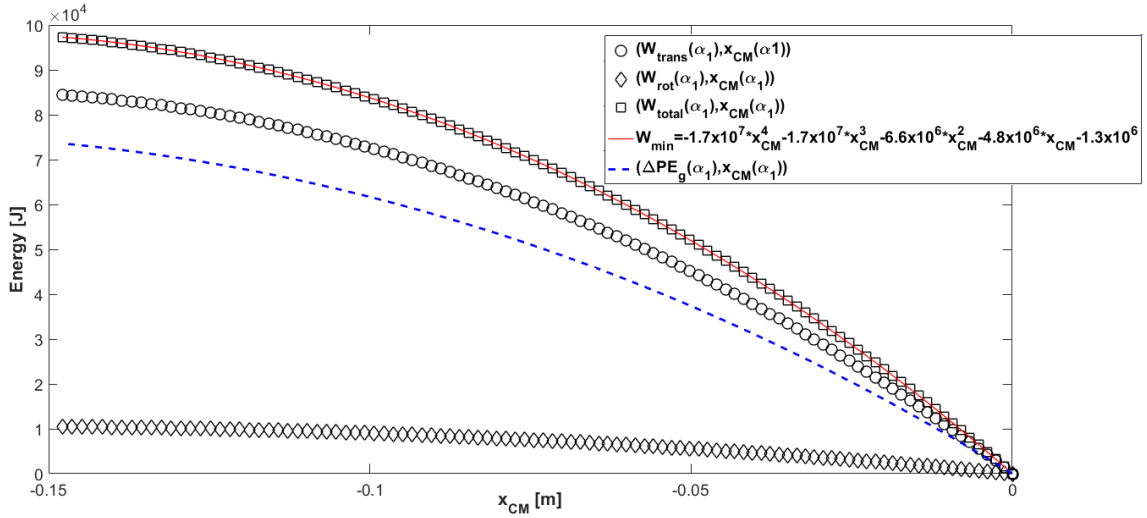

Figure 8. Parametric plot of minimum work and potential energy versus horizontal CM displacement with polynomial fit

A polynomial fit evaluation reveals that the work path is reasonably represented by

$$W_{min}(x) = C_1 x^4 + C_2 x^3 + C_3 x^2 + C_4 x + C_5 \tag{14}$$

where the constants C_i are shown in Figure 8.

3.6 Kinetic Energy

The work path, W_{min} (see Figure 8) represents the work required to maintain kinematic equilibrium along the path to collapse. An applied acceleration force, F_{app}, in excess of the static limit, F_{min}, results in the system's transition from stable to mechanical. Rigid elements and ideal hinges then require the excess energy added to the system after exceeding the stable limit be in the form of work, W_{app}, and any of this added work in excess of that required must be transformed into kinetic energy

$$\Delta KE = W_{app} - W_{req} \tag{15}$$

The required work, W_{req}, to travel from the initial position x_1 to a final position x is

$$W_{req} = W_{min}(x) - W_{min}(x_1) \tag{16}$$

If the initial kinetic energy, KE_I, is known, then with Eqns. 15 and 16 a spatial description of the final kinetic energy is obtained

$$KE_f(x) = KE_1 + F_{app}(x - x_1) - W_{min}(x) + W_{min}(x_1) \tag{17}$$

3.7 Time Domain

Kinetic energy can also be expressed in terms of translational and rotational velocities

$$KE = \frac{1}{2} m_T \boldsymbol{v}^2 + \frac{1}{2} I_{E1} \omega_{E1}^2 + \frac{1}{2} I_{E2} \omega_{E2}^2 + \frac{1}{2} I_{E3} \omega_{E3}^2 \tag{18}$$

In Eqn 18, $\boldsymbol{v}$ is the velocity vector, ω_{Ej} and I_{Ej} are the lever arm angular velocity and moment of inertia for the j^{th} element respectively. The velocity vector decomposes to

$$\boldsymbol{v} = \frac{d\boldsymbol{r}}{dt} = \frac{dx}{dt} + \frac{dy}{dt} \tag{19}$$

and the angular velocities can be expressed as

$$\omega = \frac{d\theta}{dt} \tag{20}$$

Taking the time derivatives of Eqns. 10 and 11, and utilizing Eqns. 17 through 20 generates the expression of the final kinetic energy

$$KE_f(x) = \frac{1}{2}\left[m_T \left(1 + \frac{1}{2} A_1 x + A_2\right)^2 + \sum_{i=1}^{3} m_{Ej} l_{Ei}^2 \left(\frac{1}{2} B_{1,Ej} x + B_{2,Ej}\right)^2 \right] \left(\frac{dx}{dt}\right)^2 \tag{21}$$

where m_{Ej} and l_{Ej} are the j^{th} elements mass and lever arm and the constants $B_{1,Ej}$ and $B_{2,Ej}$ are obtained from Eqn. 10 and Figure 5. The spatial description of kinetic energy, Eqn. 19, allows the isolation of variables in Eqn. 21 and the relationship between time and displacement is formed

$$t - t_0 = \int H(x)\, dx \tag{22}$$

where

$$H(x) = \sqrt{\frac{m_T\left(1+\frac{1}{2}A_1 x + A_2\right)^2 + \sum_{i=1}^{3} m_{Ei} l_{Ei}^2 \left(\frac{1}{2} B_{1,Ei} x + B_{2,Ei}\right)^2}{2KE_f(x)}} \tag{23}$$

Figure 9 shows a plot of Eqn. 23 and the numeric evaluation area for Eqn. 22 with an applied acceleration of $1.14\lambda_a$. The initial time and kinetic energy are set to zero.

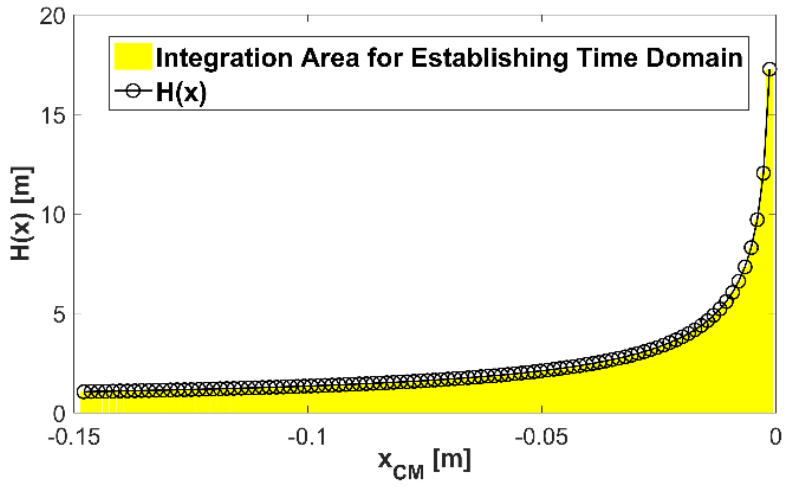

Figure 9. H(x) versus horizontal CM displacement and integration area.

Figure 10 shows the solution to Eqn. 22 and establishes the relationship between horizontal position and time. Applying a polynomial fit to the time-displacement curve reveals

$$x(t) = D_1 t^4 + D_2 t^3 + D_3 t^2 + D_4 t + D_5 \tag{24}$$

as a reasonable representation. The values of constants D_i are shown in the Fig. 10. Therefore, if the initial position and kinetic energy are known, the final displacement and kinetic energy can be calculated for the duration of a given acceleration.

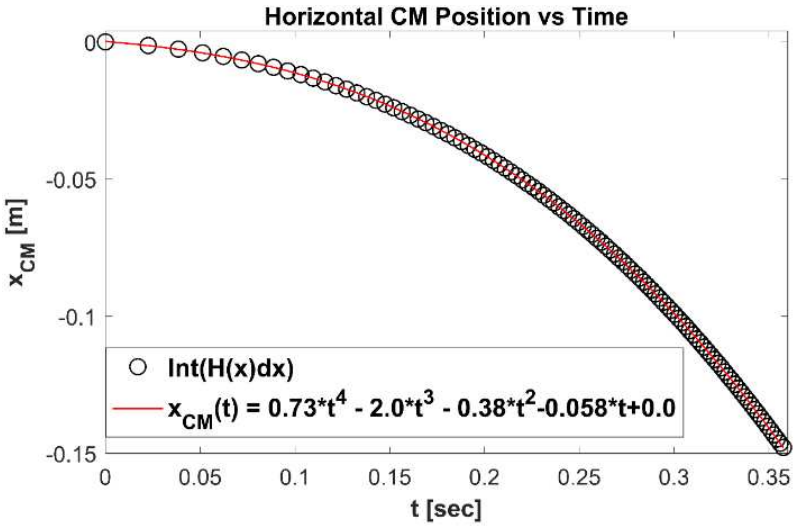

Figure 10. Horizontal CM position versus time with 4th degree polynomial fit.

4 NON-HORIZONTAL ACCELERATIONS

The expansion of the work-path approach to incorporate non-horizontal accelerations begins with the inclusion of a polar acceleration angle, θ_a, to the constant acceleration, $\lambda_a g$, and the construction of the equation set. Decomposing the acceleration multiplier produces

$$\lambda_x = \lambda_a \cos(\theta_a) \tag{25}$$

and

$$\lambda_y = \lambda_a \sin(\theta_a) \tag{26}$$

For a defined acceleration angle, the balance condition for the same arch-hinge condition as shown in Figure 1 becomes

$$[BC] = \begin{bmatrix} -1 & 0 & 1 & 0 & 0 & 0 & 0 & 0 & f_{ax1} \\ 0 & 1 & 0 & -1 & 0 & 0 & 0 & 0 & f_{ay1} \\ 0 & 0 & \Delta y_{2,1} & \Delta x_{1,2} & 0 & 0 & 0 & 0 & f_{ax1}\Delta y_{CM1,1} - f_{ay1}\Delta x_{1,CM1} \\ 0 & 0 & -1 & 0 & 1 & 0 & 0 & 0 & f_{ax2} \\ 0 & 0 & 0 & 1 & 0 & 1 & 0 & 0 & f_{ay2} \\ 0 & 0 & 0 & 0 & \Delta y_{3,2} & -\Delta x_{2,3} & 0 & 0 & f_{ax2}\Delta y_{CM2,2} - f_{ay2}\Delta x_{2,CM2} \\ 0 & 0 & 0 & 0 & -1 & 0 & 1 & 0 & f_{ax3} \\ 0 & 0 & 0 & 0 & 0 & -1 & 0 & 1 & f_{ay3} \\ 0 & 0 & 0 & 0 & 0 & 0 & \Delta y_{3,4} & -\Delta x_{3,4} & f_{ax3}\Delta y_{3,CM3} + f_{ay2}\Delta x_{3,CM3} \end{bmatrix} \tag{27}$$

The reaction and constants vectors, Eqns. 4 and 5, are unchanged for evaluating equilibrium (Eqn. 2).

4.1 Limit Line

In order to establish the limits of acceleration angles and mechanization, polar and cartesian plots of the collapse multiplier versus direction angle for the undeformed arch-hinge set shown in Figure 3 were developed (see Figure 11). For both plots a full 360° rotation was evaluated at 1° intervals with no admissibility evaluation. From the cartesian plot the limits of admissible angles (positive λ_a) are clearly identified as 87.5° through 267.5°. From the polar plot a limit line is established and interestingly the negative multipliers exactly overlay the same line. This limit line creates the boundary condition of mechanism formation from 2D accelerations applied to the given mechanism.

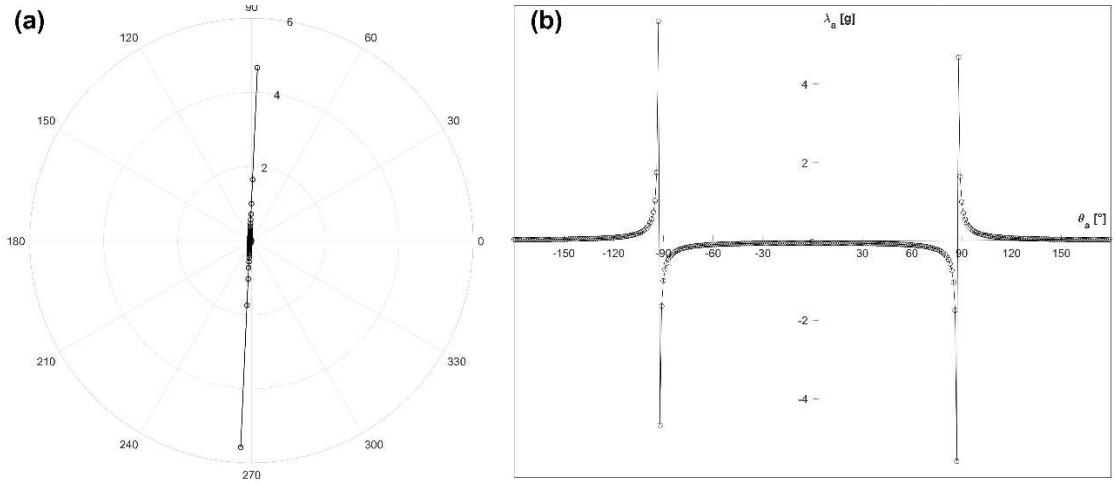

Figure 11. (a) Polar and (c) cartesian plots of the collapse multiplier versus acceleration vector angle

4.1.1 Limit Line and Static Deformations

Figure 12 shows the limit line plots for α_1 deformations of 0°, 4°, 8° and 12° applied to the arch-hinge condition in Figure 3. Interestingly, the deformation of the arch causes the limit line to pivot towards vertical about the point 1 at 90°. Additionally, the loss of admissibility at 12° is identified by the limit line crossing the vertical origin. The pivot point is a shift from gravity's inclusion in the constants vector.

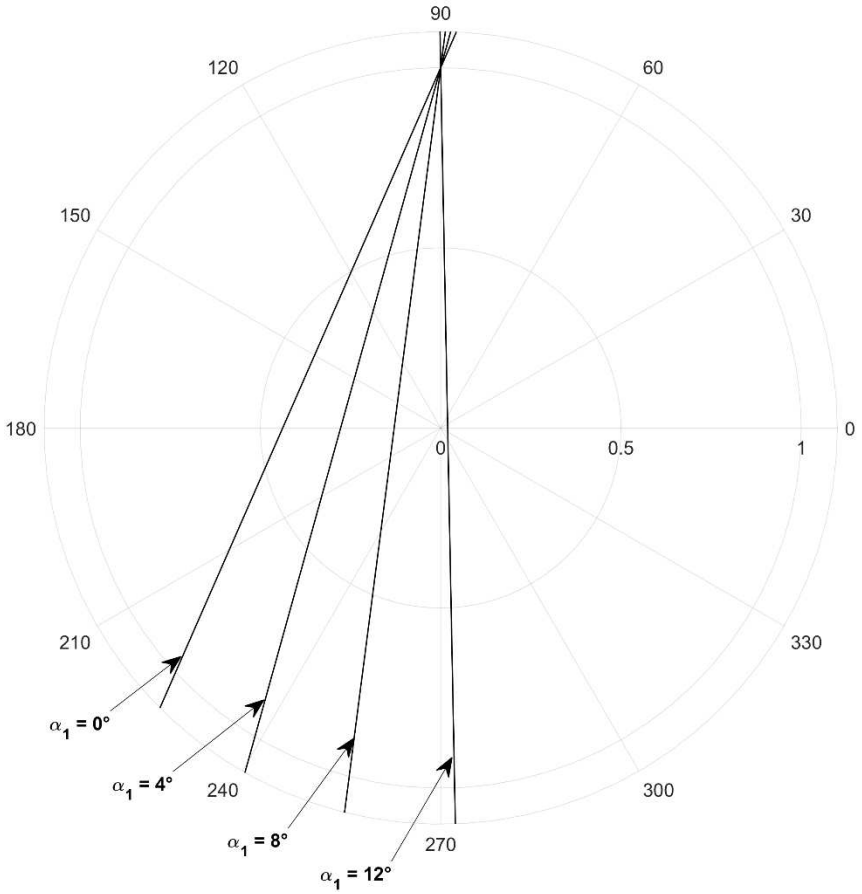

Figure 12. Acceleration limit lines for α_1 deformations of 0°, 4°, 8° and 12°

4.2 Work Path

The inclusion of a vertical force introduces a vertical component of work

$$W_{app} = \int F_x dx + \int F_y dy \tag{28}$$

but utilizing Eqn. 11 and its derivative with respect to x allows the work to be rewritten in terms of x

$$W = \int \left[F_x + F_y \left(\frac{1}{2} B_1 x + B_2 \right) \right] dx \tag{29}$$

Figure 13 shows the calculated minimum work paths for various acceleration angles within the established limits. From this figure it can be seen that the required work decreases with the angle.

In terms of cartesian coordinates, the more negative the vertical component of acceleration the greater the required work. In fact, for the angle of 90°, the multiplier is 1.0 and the translational work required to carry the arch to collapse is identical to the change in potential energy (see Figure 14). This translational equivalence provides a validation of the established work-path calculation. The rotational work transitions from working against the motion to working with the motion as the acceleration angle approaches positive vertical (see Figure 14). Figure 1This rotational work transformation results in the required work being less than the change in potential energy for acceleration angles between 90° and 97° for the arch-hinge set under evaluation (see Figure 13). Additionally, Eqn. 14 holds with varying constants for all work paths evaluated.

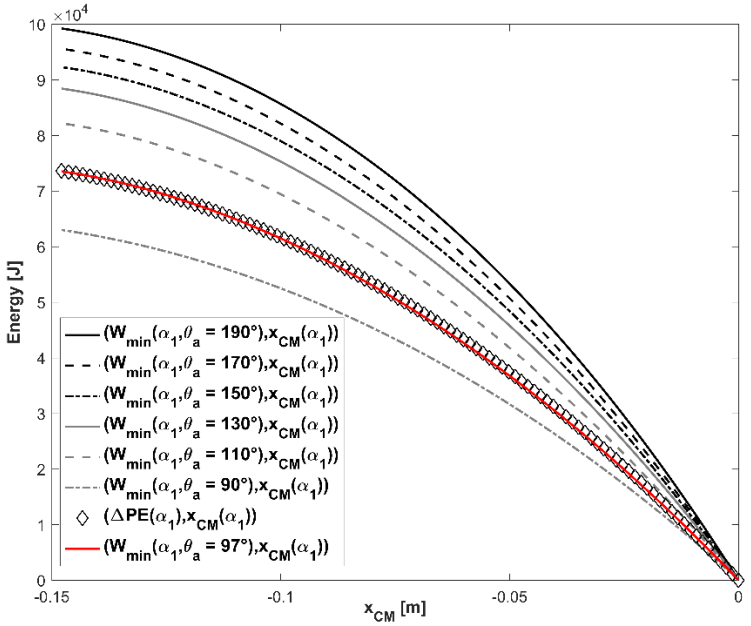

Figure 13. Parametric plots of minimum work versus horizontal displacement for different acceleration vector angles, θ_a

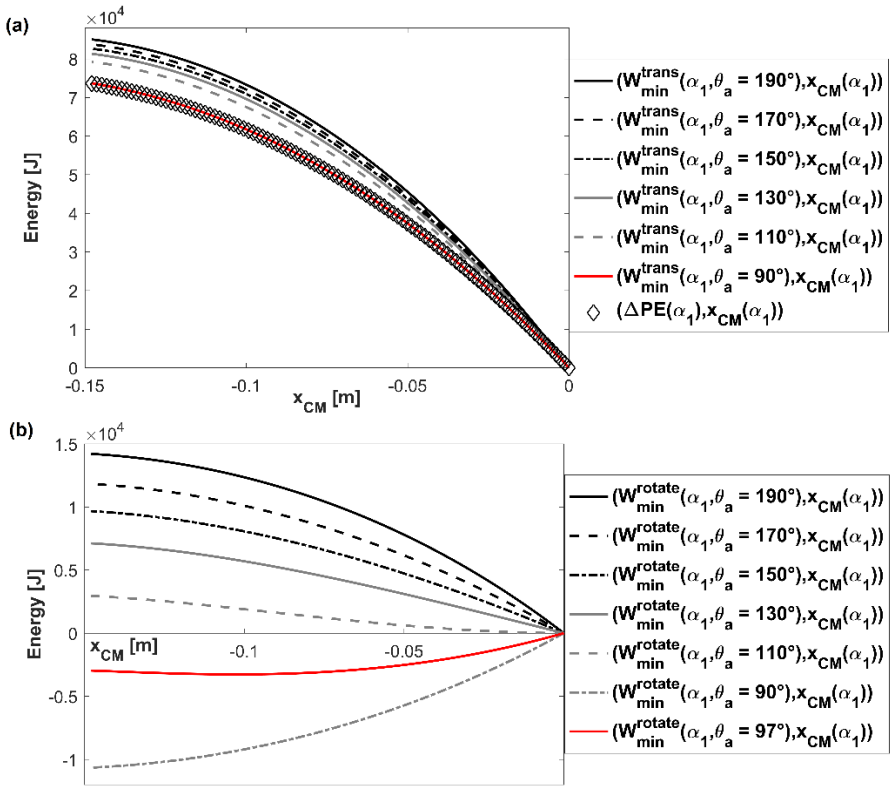

Figure 14. Parametric Plots of the minimum (a) translational and (b) rotational work for various acceleration angles

4.3 Kinetic Energy and Time Domain

With the inclusion of the vertical component of acceleration, the final displacement based kinetic energy equations becomes

$$KE_f(x) = KE_1 + F_x(x - x_1) + F_y\left[\frac{1}{2}B_1(x^2 - x_1^2) - B_2(x - x_1)\right] - W_{min}(x) + W_{min}(x_1) \qquad (30)$$

Therefore, the time domain equations (Eqns. 22 and 23) hold. Additionally, since Eqn. 14 holds for acceleration vector angles within the limits, the time-displacement equation (Eqn. 24) and the procedure of obtaining its constants holds. Consequently, a simple methodology is established for evaluating the onset of a defined mechanism and obtaining the resulting time-displacement domain for any constant 2D acceleration.

5 Dynamic Analysis Procedure

Consider an undeformed and stable arch subjected to a time dependent acceleration sequence which crosses the limit line at time t_1. Assuming constant acceleration, allows the formulation of the kinetic energy equation (Eqn. 28) and the time-displacement equation (Eqn. 24). At time t_2 the acceleration changes. Applying t_2-t_1 to Eqn. 24 establishes the displacement x_2 at t_2. Having the displacement then allows the kinetic energy at time t_2 to be calculated with Eqn. 30. Then the final position and kinetic energy from the first acceleration become the initial conditions for the

second acceleration value. In this manner, the arch can be dynamically propagated forward in time.

5.1 Kinematic Condition and the Limit Line

If at time t_2 the displacement of the arch exceeds the admissible deformation limit established through kinematic equilibrium, then the arch has collapsed. Otherwise, the arch is in a kinematic state. In this kinematic state, the effects of the second acceleration value between t_2 and t_3 depend on the limit line. Acceleration vectors that exceed the limit line will increase kinetic energy and consequently the rate of deformation towards collapse. Accelerations less than the limit line result in the developed kinetic energy being spent to propagate the arch forward. If zero kinetic energy is reached within the kinematic state, then the motion and work are reversed.

5.2 Forward Facing Motion

Establishing the $H(x)$ function (Eqn. 23) for obtaining the time domain (Eqn. 22) requires a positive non-zero kinetic energy. Reversing motion and releasing the stored energy generates a negative kinetic energy with respect to Eqn. 30. Therefore, the motion must be considered as forward facing which is achieved by the absolute value of the negative limits of the kinetic energy equation (Eqn. 30).

5.3 Crossing the Origin and the Coefficient of Restitution

With the reversal of motion from insufficient acceleration to cause collapse the arch is propagated towards its undeformed condition. When that condition is reached an impact at the mechanical joints will occur if the kinetic energy is greater than zero. The impact will result in a dissipation of energy for a finite duration of time. The Coefficient of Restitution (COR) is the standard parameter to define energy loss from one of three models known as kinematic, kinetic and energetic (Ahmad, Ismail and Mat, 2016). Newton's kinematic model

$$COR = \frac{KE_f}{KE_i} \tag{31}$$

directly aligns itself with the work-path model considered here. Establishing an accurate COR for a specific condition is outside the current scope of work, but the incremental structure of the dynamic analysis model allows the impact to be isolated by timesteps and the COR applied. The importance is that a COR can be easily controlled in the transition between the two hinge sets that define motion.

If sufficient kinetic energy exists and the impact is not plastic (i.e. COR = 0), then the hinge positions switch joint limits and the reversed mechanism is established. The limit line, deformation path and minimum work-path are switched to the new mechanism. The reduced kinetic energy and next acceleration vector are set and the evaluation continues.

5.4 COMBINING CONDITIONS

The dynamic propagation procedure of the hinge-controlled masonry arch generates two deformation paths. Each deformation path has two directions of motion for a total of four forward facing motion conditions. Lastly, the kinematic condition has three boundary conditions: two that indicate collapse and the stable state where impact occurs. Figure 15 shows the combination of these conditions into a flowchart that represents the dynamic analysis procedure. For each time step in the defined acceleration sequence the limit line is established and used to evaluate the work condition. The established condition with the existing kinetic energy and position generate a final position and kinetic energy. The reversal of kinetic energy switches the motion direction. Crossing the origin triggers the COR and switches the hinge set. This process is repeated until the end of the acceleration sequence or a maximum allowed displacement is reached.

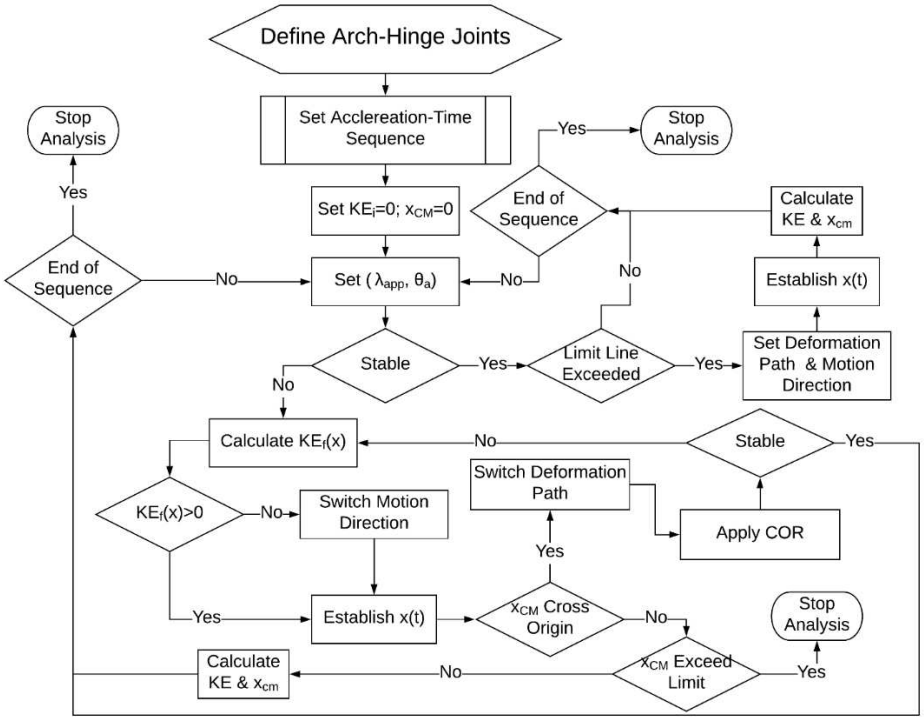

Figure 15. Flowchart of the dynamic analysis procedure.

6 HALF CYCLE COLLAPSE AND CONSERVATION OF ENERGY

The developed dynamic modelling procedure was formulated from the principles of energy conservation, equivalent systems through parametric plotting, and the path independence of conservative work. The equivalent systems were directly defined through the centroid calculations for fixed rotations of hinge H_1. These centroid deformations established deformation paths and subsequently work-paths. The minimum work-paths were validated by the equivalence of work and potential energy for vertical acceleration and the zero net torque for all kinematically admissible equilibrium conditions. Therefore, the final validations for the analysis

structure are Oppenheim's half-cycle collapse line benchmark and the conservation of energy (Oppenheim, 1992).

The Oppenheim arch geometry and the hinge reversal from fixed mechanical joints is shown in Figure 16 (Oppenheim, 1992). These two configurations establish the dynamic model for the arch.

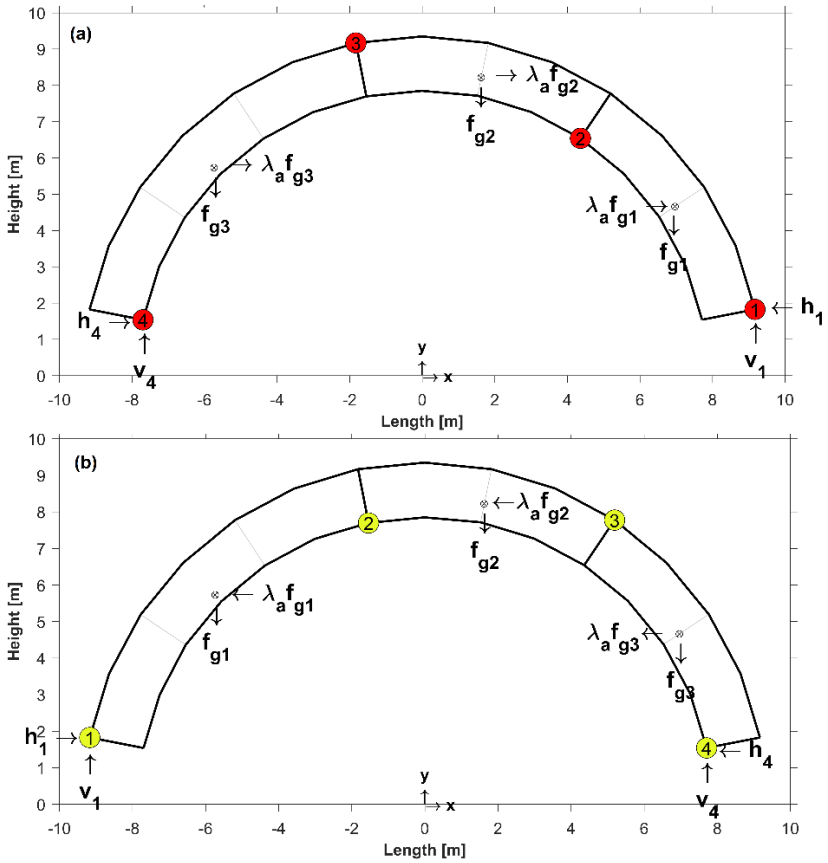

Figure 16. Oppenheim arch geometry with the (a) original hinge geometry and (b) the hinge reversal from defined joints

Figure 17 shows a graphical display created to monitor the propagation of a dynamic sequence. This graphical display consists of the arch represented in element form, the acceleration limit tracker, the CM position tracker and the applied acceleration sequence. The arch plot shows the arches geometric condition through the dynamic sequence. The acceleration limit tracker identifies the applied acceleration and kinematic condition at each time step. For the limit lines and applied acceleration, red indicates a condition promoting collapse and blue a condition promoting recovery.

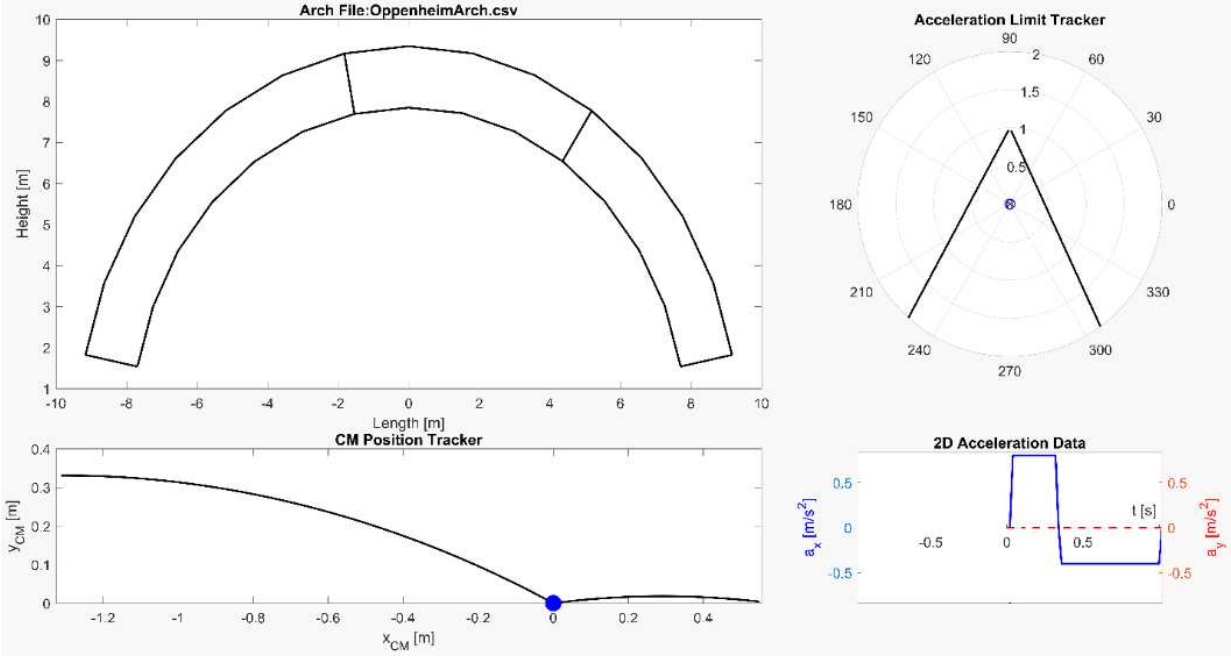

Figure 17. Dynamic monitoring display at time zero for a two-step pulse

Figure 18 shows three examples of the motion conditions through the propagation of the horizontal two-step pulse. First, the acceleration and kinematic motion are both propagating towards collapse, then the acceleration drops below the limit line and the net-work is against collapse. Lastly in Fig. 18 both motion and acceleration are driving the arch towards its original configuration. If the deformation of the arch reaches or exceeds the limit established through kinematic admissibility, then the arch geometry and CM tracker both turn red and the evaluation is stopped. Figure 19 shows this failure condition for a two-step pulse in excess of recovery.

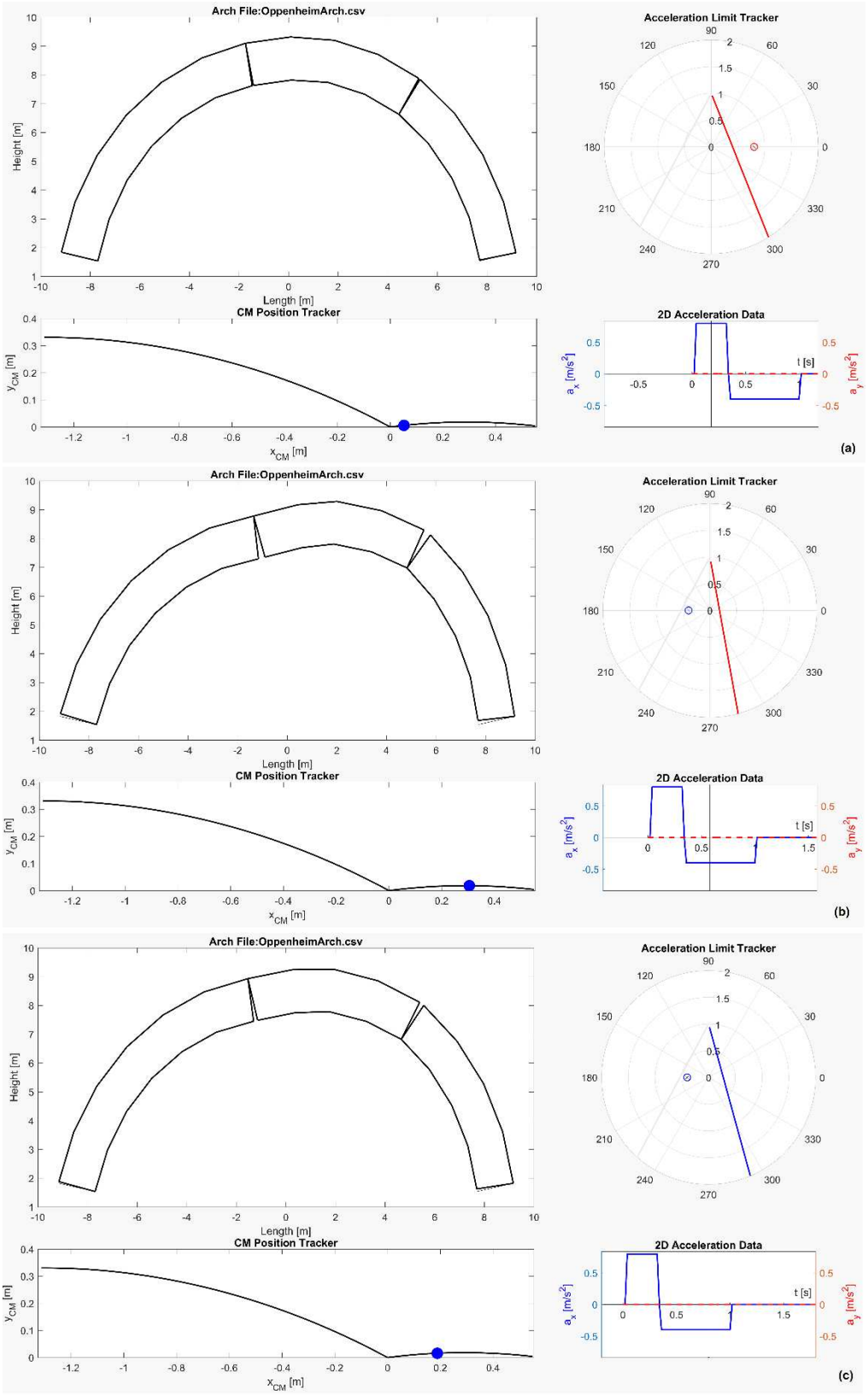

Figure 18. Dynamic propagation of the two-step pulse with (a) acceleration and motion propagating towards collapse, (b) acceleration working towards recovery, and (c) motion and acceleration towards recovery

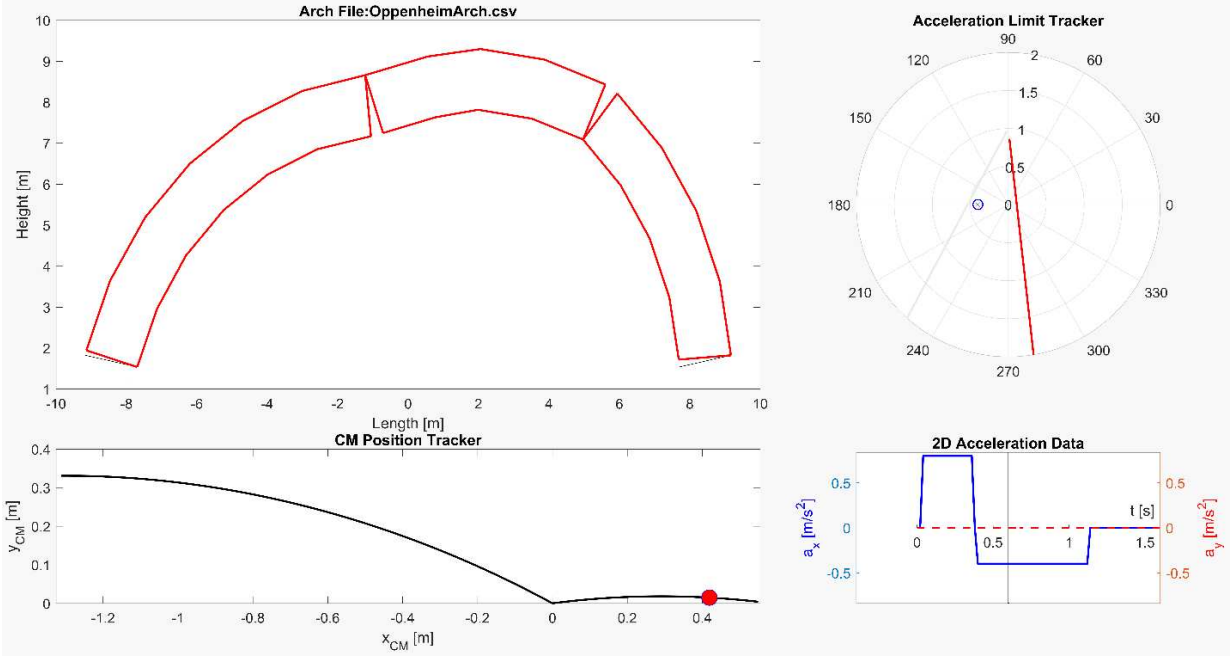

Figure 19. Identified collapse in the dynamic propagation

6.1 Half Cycle Collapse

For the half-cycle collapse evaluation, the Oppenheim two-step acceleration pulse was applied (Oppenheim, 1992). For each acceleration amplitude, the pulse time was continually increased by 0.02 seconds until a collapse was obtained (see Figure 19). The resulting half-cycle failure domains from the described work-path approach and Oppenheim's original results are shown in Figure 20. This comparison of results show an increase in static capacity from the upper bound limit of the work-path approach and a small decrease in the recoverable impulse duration. Nonetheless, the behavior of the arche's half-cycle failure is captured by the work-path approach and with more conservative impulse duration limits.

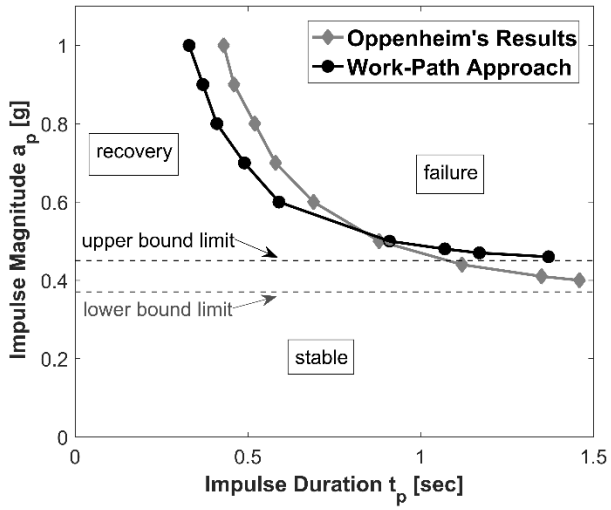

Figure 20. Half-cycle failure domain comparison for the two-step pulse analysis of the Oppenheim arch (Oppenheim, 1992)

Repeating the half-cycle collapse evaluation with constant vertical accelerations generates the failure domains shown in Figure 21. The inclusion of the vertical acceleration has the expected effect of changing the static limit of its horizontal counterpart. Additionally, the behavior of the half-cycle failure is maintained for all the shown conditions minus the vertical acceleration of 0.9g. As previously discussed, this strong vertical acceleration has the effect of reversing the rotational work and minimizing the window of recovery for weak horizontal pulses. This phenomenon is consistent with the observations of the work paths shown in Figure 14 and diminishes as the horizontal acceleration's magnitude increases.

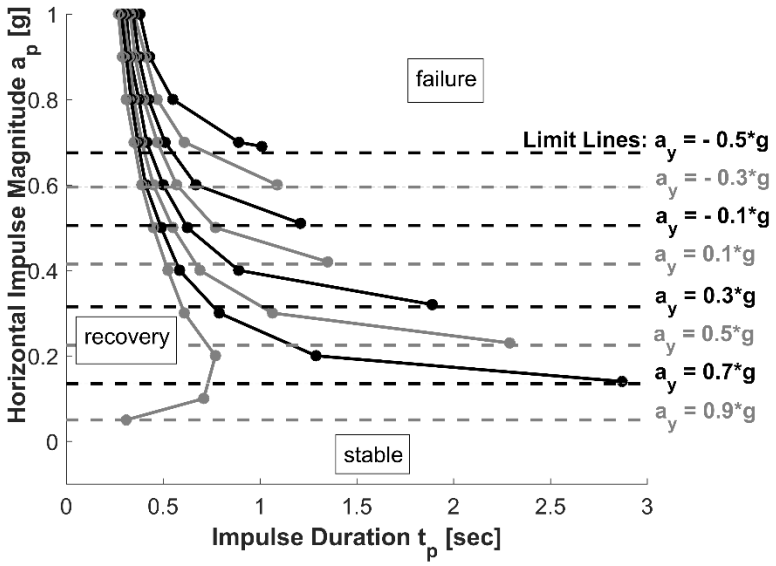

Figure 21. Half-cycle failure domains for various vertical accelerations with a horizontal pulse

6.2 CONSERVATION OF ENERGY

Conservation of energy was evaluated by the application of a 0.55g magnitude acceleration with various vector angles for 0.5 seconds and then removed. The arch was set in free motion for the remaining duration of the 20 second sequence with perfectly elastic impacts (i.e. COR = 1) and instantaneous mechanism switches. The timesteps were set at 0.02 seconds.

The limit line for rightward motion in Figure 17 identifies the vector angle limits for mechanization from a 0.55g magnitude acceleration as $-17° \leq \theta_a \leq 65°$, and thus acceleration angles between -10° and 50° were selected for evaluation. For each evaluation the horizontal CM displacement and kinetic energy were recorded at each timestep. Figure 22 shows examples of the displacement and kinetic energy plots for the first ten seconds with applied acceleration angles of -10°, 0° and 10°. From this figure the application of the acceleration and the periodic nature of free motion are observed with two distinct half-cycles corresponding to the two mechanism geometries. Additionally, the displacements and kinetic energies are out phase as expected.

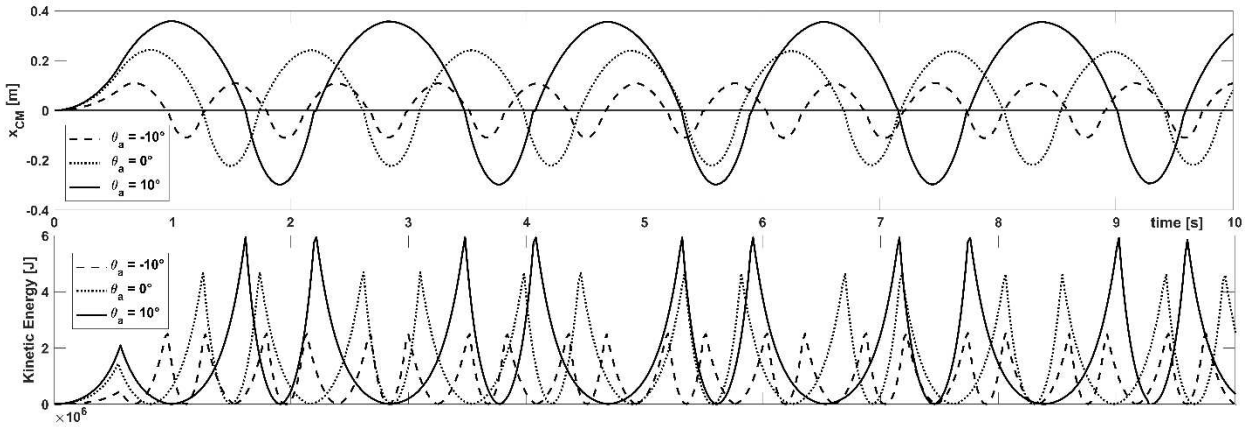

Figure 22. Horizontal CM displacement and kinetic energy versus time for applied acceleration pulse

Figure 23 shows the percentage of energy loss between the first and last cycle of recorded motion for each acceleration angle tested. The average energy loss was 4.4% over the 20 second evaluation for all the tests and the loss of energy never exceeded 10% for any single analysis. Therefore, it can be reasonably argued that energy is conserved for the ideal conditions.

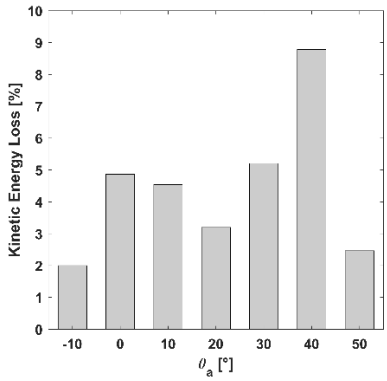

*Figure 23. Kinematic energy loss versus applied acceleration angle for a 0.55*g magnitude acceleration applied for 0.5 seconds*

Lastly, Figure 24 shows the peak displacement, the time of peak displacement, and the maximum kinetic energy for each of the applied acceleration angles. From each of these plots, the sensitivity of the arches response to the acceleration vector angle is clear and the vector angle of 20° is identified as the most kinematically significant angle for the single pulse applied to the given arch-hinge configuration.

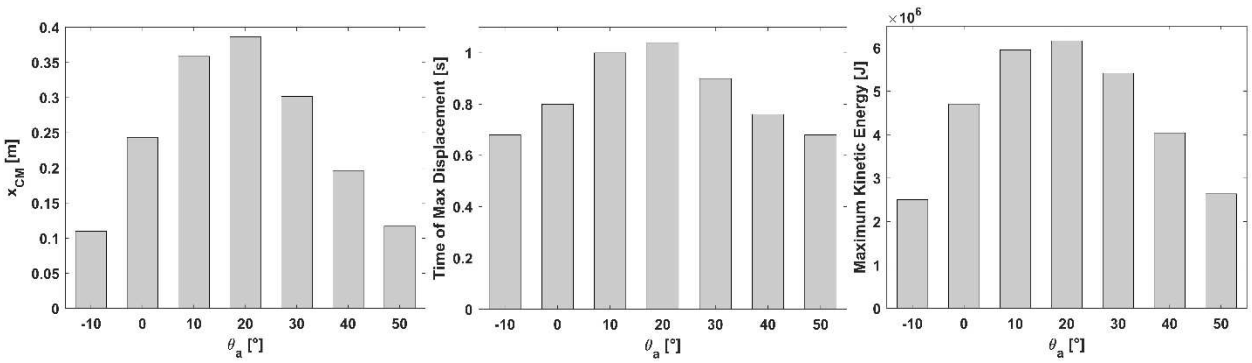

*Figure 24. Maximum horizontal CM position, time of maximum displacement, and maximum kinetic energy versus applied acceleration angle for a 0.55*g magnitude acceleration applied for 0.5 seconds*

7 CONCLUSIONS

Engineering efficiency is paramount for the introduction of novel systems and formats of analysis. The fundamentals of the masonry arch have the potential to create an advantageous structural system for modern structural design and construction. This work extends an accessible and efficient analysis platform built off of the kinematic equilibrium approach to LA and the SDOF nature of a hinge-controlled arch to the dynamic modelling of applied two-dimensional acceleration vectors. Utilizing ideal conditions, the work path and ultimately the time domain were established for applied 2D accelerations and used to formulate the dynamic time incremental analysis structure based upon the assumption of constant acceleration for each time step. The time domain and kinetic energy equations were then coupled with the finite set of motions and impacts to establish the modelling structure.

The dynamic modelling structure was then evaluated for its half cycle collapse and conservation of energy. From the tests, the behavior of the analyzed arch was validated for ideal conditions. Additionally, the sensitivities of the accelerations angle are clearly identified for the geometric condition.

With the inclusion of the dynamic state, the foundation for a complete and comprehensive analysis structure has been formulated for hinge-controlled masonry arches. This brings the utilization of structural masonry one step closer to implementaion. The focus must now turn to experimental testing and the incorporation of non-ideal conditions.

8 REFERENCES

Ahmad, M., Ismail, K. A. and Mat, F. (2016) 'IMPACT MODELS AND COEFFICIENT OF RESTITUTION: A REVIEW', *Journal of Engineering and Applied Sciences*, 11(10), pp. 6549–6555. Available at: www.arpnjournals.com (Accessed: 14 May 2019).

Alexakis, H. and Makris, N. (2014) 'Limit equilibrium analysis and the minimum thickness of circular masonry arches to withstand lateral inertial loading', *Archive of Applied Mechanics*, 84(5), pp. 757–772. doi: 10.1007/s00419-014-0831-4.

Angelillo, M. (ed.) (2014) *Mechanics of Masonry Structures*. Vienna: Springer Vienna (CISM International Centre for Mechanical Sciences). doi: 10.1007/978-3-7091-1774-3.

Clemente, P. (1998) 'Introduction to dynamics of stone arches', *Earthquake Engineering & Structural Dynamics*. John Wiley & Sons, Ltd, 27(5), pp. 513–522. doi: 10.1002/(SICI)1096-9845(199805)27:5<513::AID-EQE740>3.0.CO;2-O.

DeJong, M. J. (Matthew J. (2009) *Seismic assessment strategies for masonry structures*. Massachusetts Institute of Technology.

DeJong, M. J. and Dimitrakopoulos, E. G. (2014) 'Dynamically equivalent rocking structures', *Earthquake Engineering & Structural Dynamics*. John Wiley & Sons, Ltd, 43(10), pp. 1543–1563. doi: 10.1002/eqe.2410.

Dimitri, R., De Lorenzis, L. and Zavarise, G. (2011) 'Numerical study on the dynamic behavior of masonry columns and arches on buttresses with the discrete element method', *Engineering Structures*. Elsevier, 33(12), pp. 3172–3188. doi: 10.1016/J.ENGSTRUCT.2011.08.018.

Dimitri, R. and Tornabene, F. (2015) 'A parametric investigation of the seismic capacity for masonry arches and portals of different shapes', *Engineering Failure Analysis*. Pergamon, 52, pp. 1–34. doi: 10.1016/J.ENGFAILANAL.2015.02.021.

Fanning, P. J. *et al.* (2005) 'Load testing and model simulations for a stone arch bridge', *Bridge Structures*. Taylor & Francis , 1(4), pp. 367–378. doi: 10.1080/15732480500453532.

Gaetani, A. *et al.* (2017) 'Shaking table tests and numerical analyses on a scaled dry-joint arch undergoing windowed sine pulses', *Bulletin of Earthquake Engineering*. Springer Netherlands, 15(11), pp. 4939–4961. doi: 10.1007/s10518-017-0156-0.

Gilbert, M. and Melbourne, C. (1994) 'Rigid-Block Analysis of Masonry Structures', *Structural Engineer*, 72(21), pp. 356–361.

Hendry, A. W. (1998) *Structural Masonry*. 2nd edn. London: Macmillan Education UK. doi: 10.1007/978-1-349-14827-1.

Heyman, J. (1969) 'The safety of masonry arches', *International Journal of Mechanical Sciences*. Pergamon, 11(4), pp. 363–385. doi: 10.1016/0020-7403(69)90070-8.

Housner, G. W. (1963) 'The behavior of inverted pendulum structures during earthquakes', *Bulletin of the Seismological Society of America*. Seismological Society of America, 53(2), pp. 403–417. Available at: https://pubs.geoscienceworld.org/ssa/bssa/article-abstract/53/2/403/116143 (Accessed: 21 May 2019).

Huerta, S. (2005) 'The use of simple models in the teaching of the essentials of masonry arch behaviour', in Mochi, G. (ed.) *Theory and practice of constructions: knowledge, means and models. Didactis and research experiences*. Ravenna, Italia: Fondazione Flaminia, pp. 747–761. Available at: http://oa.upm.es/570/.

Kollár, L. P. and Ther, T. (2019) 'Numerical model and dynamic analysis of multi degree of freedom masonry arches', *Earthquake Engineering and Structural Dynamics*, (January), pp. 709–

730. doi: 10.1002/eqe.3158.

De Lorenzis, L., DeJong, M. and Ochsendorf, J. (2007) 'Failure of masonry arches under impulse base motion', *Earthquake Engineering & Structural Dynamics*. John Wiley & Sons, Ltd, 36(14), pp. 2119–2136. doi: 10.1002/eqe.719.

De Luca, A., Giordano, A. and Mele, E. (2004) 'A simplified procedure for assessing the seismic capacity of masonry arches', *Engineering Structures*. Elsevier, 26(13), pp. 1915–1929. doi: 10.1016/J.ENGSTRUCT.2004.07.003.

Ochsendorf, J. (2002) *Collapse of masonry structures*. Univeristy of Cambridge. doi: 10.17863/CAM.14048.

Oppenheim, I. J. (1992) 'The masonry arch as a four-link mechanism under base motion', *Earthquake Engineering & Structural Dynamics*. John Wiley & Sons, Ltd, 21(11), pp. 1005–1017. doi: 10.1002/eqe.4290211105.

Pelà, L., Aprile, A. and Benedetti, A. (2009) 'Seismic assessment of masonry arch bridges', *Engineering Structures*. Elsevier, 31(8), pp. 1777–1788. doi: 10.1016/J.ENGSTRUCT.2009.02.012.

Pelà, L., Aprile, A. and Benedetti, A. (2013) 'Comparison of seismic assessment procedures for masonry arch bridges', *Construction and Building Materials*. Elsevier, 38, pp. 381–394. doi: 10.1016/J.CONBUILDMAT.2012.08.046.

Sarhosis, V. *et al.* (2016) *Computational modeling of masonry structures using the discrete element method*. Available at: https://books.google.it/books?hl=en&lr=&id=RD9nDAAAQBAJ&oi=fnd&pg=PP1&dq=Sarhosis+V,+Bagi+K,+Lemos+JV,+Milani+G+(2016a)+Computational+modeling+of+masonry+structures+using+the+discrete+element+method.+IGI+Global,+Hershey&ots=H_xkk5WNYx&sig=gWt4iVubbgiw0wPL (Accessed: 26 February 2019).

Sarhosis, V., Santis, S. De and de Felice, G. (2016) 'A review of experimental investigations and assessment methods for masonry arch bridges', *Structure and Infrastructure Engineering*. Taylor & Francis, 12(11), pp. 1439–1464. doi: 10.1080/15732479.2015.1136655.

Stockdale, G. L. (2012) *Generalized Processing of Fbg / Frp Strain Data for Structural Health Monitoring*. University of Hawaii at Manoa.

Stockdale, G. L. (2016) 'Reinforced stability-based design: a theoretical introduction through a mechanically reinforced masonry arch', *International Journal of Masonry Research and Innovation*, 1(2), pp. 101–142. doi: 10.1504/IJMRI.2016.077469.

Stockdale, G. L. *et al.* (2018) 'Kinematic collapse load calculator: Circular arches', *SoftwareX*. doi: 10.1016/j.softx.2018.05.006.

Stockdale, G. L. and Milani, G. (2018) 'Interactive MATLAB-CAD limit analysis of horizontally loaded masonry arches', in *10th IMC Conference Proceedings*. Milan: International Masonry Society, pp. 298–306.

Stockdale, G. L. and Milani, G. (2019) 'Diagram based assessment strategy for first-order

analysis of masonry arches', *Journal of Building Engineering*. Elsevier, 22, pp. 122–129. doi: 10.1016/J.JOBE.2018.12.002.

Stockdale, G., Sarhosis, V. and Milani, G. (2019a) 'Finite hinge stiffness and its effect on the capacity of a dry-stack masonry arch subjected to hinge control', in. Bologna: Key Engineering Materials, pp. 1–8.

Stockdale, G., Sarhosis, V. and Milani, G. (2019b) 'Seismic capacity and multi-mechanism analysis for dry-stack masonry arches subjected to hinge control', *Bulletin of Earthquake Engineering*. Springer Netherlands, (0123456789). doi: 10.1007/s10518-019-00583-7.

Tralli, A., Alessandri, C. and Milani, G. (2014) 'Computational Methods for Masonry Vaults: A Review of Recent Results', *The Open Civil Engineering Journal*, 8(1), pp. 272–287. doi: 10.2174/1874149501408010272.